

Article

Experimental Hydrothermal Alteration of Rhyolite and Andesite at 325 °C and 300 Bar: Implications for a Potential Role of Volcanic Glass in the Fluid Composition in the Okinawa Trough

Masafumi Saitoh ^{1,2,3,*}, Takazo Shibuya ^{1,2,4} , Takuya Saito ⁴, Junji Torimoto ¹, Hisahiro Ueda ⁵, Tomoki Sato ⁶  and Katsuhiko Suzuki ^{1,2,7} 

- ¹ Ore Genesis Research Unit, Project Team for Development of New-Generation Research Protocol for Submarine Resources, Japan Agency for Marine-Earth Science & Technology (JAMSTEC), 2-15 Natsushima-cho, Yokosuka 237-0061, Japan; takazos@jamstec.go.jp (T.S.); jtori@jamstec.go.jp (J.T.); katz@jamstec.go.jp (K.S.)
 - ² Research and Development (R&D) Center for Submarine Resources, Japan Agency for Marine-Earth Science and Technology (JAMSTEC), 2-15 Natsushima-cho, Yokosuka 237-0061, Japan
 - ³ The University Museum, The University of Tokyo, Hongo, Tokyo 113-0033, Japan
 - ⁴ Institute for Extra-Cutting-Edge Science and Technology Avant-Garde Research (X-Star), Super-Cutting-Edge Grand and Advanced Research (SUGAR) Program, Japan Agency for Marine-Earth Science and Technology (JAMSTEC), Natsushima-cho, Yokosuka 237-0061, Japan; sai-tak@jamstec.go.jp
 - ⁵ Department of Chemistry, Gakushuin University, 1-5-1 Mejiro, Toshima, Tokyo 171-8588, Japan; 20229032@gakushuin.ac.jp
 - ⁶ Volcanoes and Earth's Interior Research Center (VERC), Research Institute for Marine Geodynamics (IMG), Japan Agency for Marine-Earth Science and Technology (JAMSTEC), 2-15 Natsushima-cho, Yokosuka 237-0061, Japan; t-sato@jamstec.go.jp
 - ⁷ Research Institute for Marine Resources Utilization (MRU), Submarine Resources Research Center (SRRC), Japan Agency for Marine-Earth Science and Technology (JAMSTEC), 2-15 Natsushima-cho, Yokosuka 237-0061, Japan
- * Correspondence: msaitoh@um.u-tokyo.ac.jp



Citation: Saitoh, M.; Shibuya, T.; Saito, T.; Torimoto, J.; Ueda, H.; Sato, T.; Suzuki, K. Experimental Hydrothermal Alteration of Rhyolite and Andesite at 325 °C and 300 Bar: Implications for a Potential Role of Volcanic Glass in the Fluid Composition in the Okinawa Trough. *Minerals* **2024**, *14*, 259. <https://doi.org/10.3390/min14030259>

Academic Editors: Federica Zaccarini, Gabriella B. Kiss and Tamás Sági

Received: 20 January 2024

Revised: 24 February 2024

Accepted: 26 February 2024

Published: 29 February 2024



Copyright: © 2024 by the authors. Licensee MDPI, Basel, Switzerland. This article is an open access article distributed under the terms and conditions of the Creative Commons Attribution (CC BY) license (<https://creativecommons.org/licenses/by/4.0/>).

Abstract: The experimental study of water–rock reactions under high-temperature and -pressure conditions is a useful approach to constrain controlling factors of the fluid composition in a natural hydrothermal system. Previous studies have focused mainly on the mid-ocean ridge fields, and the hydrothermal alteration of intermediate-to-felsic rocks has been less emphasized despite its potential importance in the fluid chemistry in an arc/back-arc basin setting. We examined the alteration processes of fresh rhyolite and andesite rocks collected from the middle and southern Okinawa Trough, respectively, at 325 °C and 300 bar (the estimated condition at the reaction zone in the fields), especially focusing on the behavior of silica between the solid and liquid phases. The experimental fluids are characterized by the high Si concentration up to 30 mM, indicating the substantial dissolution of volcanic glass in the analyzed rocks. The high Si concentration in the fluids was presumably buffered by amorphous silica, precipitated from the fluids as a precursor of hydrothermal quartz, during the experiments. Our results emphasize a previously overlooked role of volcanic glass/amorphous silica in the fluid composition in the Okinawa Trough and are consistent with the previous model of pumice replacement mineralization for the SMS deposit formation in the trough.

Keywords: intermediate-to-felsic volcanic rocks; the Okinawa Trough; volcanic glass; hydrothermal alteration; equilibrium; SMS deposit formation

1. Introduction

Seafloor hydrothermal systems are developed mostly at the spreading or rifting center of mid-ocean ridge (MOR) and arc/back-arc (ABA) hydrothermal fields (e.g., [1]). In a hydrothermal system, seawater generally recharges into the subseafloor crust and is heated

by a deep magma chamber. The subseafloor hydrothermal fluid is compositionally changed in the reaction/discharge zone by several processes such as reactions with surrounding rocks and sediments, inputs of magmatic volatiles, and phase separation, under high-temperature and -pressure conditions [2]. The fluid eventually rises in the oceanic crust and is discharged from the seafloor and mixed with ambient cold seawater around the seafloor.

Previous studies have documented systematic differences in the fluid composition between the MOR and ABA hydrothermal fields [3,4]. These differences could be basically attributed to the difference in environmental and tectonic factors between the MOR and ABA fields, such as water depth and reacted rock type [1,5]. For example, in the MOR systems, the subseafloor hydrothermal fluids react mainly with mid-ocean ridge basalts as well as minor ultramafic rocks and offshore sediments [6]. In contrast, in the ABA systems, the fluids react with various kinds of rocks (including basalt, andesite, dacite, and rhyolite) and sediments, with generally larger inputs of magmatic volatiles and a larger influence of phase separation compared to in the MOR systems [5]. The fluid composition in the ABA systems is therefore generally characterized by wide variations compared to in the MOR systems.

The observational study of water–rock reactions under high-temperature and -pressure conditions in a simple experimental system has been a useful approach to constrain the controlling factors of fluid composition in a complex natural hydrothermal system (e.g., [7]). Previous experimental studies have focused mainly on the MOR systems and examined hydrothermal alteration processes of mafic and ultramafic rocks [7–12]. These experiments have basically reproduced the fluid composition and alteration mineralogy observed in the natural MOR systems [6] and have illustrated that the fluid composition is mainly controlled by water–rock reactions and fluid–mineral equilibria in the reaction zone in the systems (e.g., [5,13,14] and references therein).

In contrast, the experimental hydrothermal alteration of intermediate-to-felsic rocks has been less emphasized despite its potentially important role in the fluid chemistry in the ABA fields. Hajash and Chandler (1981) examined hydrothermal alteration of various rock types including rhyolite, andesite, basalt, and peridotite by reaction with natural seawater at 200–500 °C and 1000 bar [15]. They reported the formation of hydrous Mg-silicate and anhydrite, although their experiment intervals were only two weeks. Shiraki et al. (1987) examined the hydrothermal alteration of rhyolite and andesite with natural seawater at 300 °C and 1000 bar, using Dickson-type equipment [16]. They found K enrichment and Mg depletion in the fluids and proposed two-stage alteration processes during the Kuroko-type mineralization. Chiba (1995) conducted chemical modeling calculations for the hydrothermal alteration of basalt, andesite, and rhyolite, assuming fluid–mineral equilibria in the system [17]. He illustrated that the rock type is an important controlling factor on the fluid composition. Ogawa et al. (2005) examined the hydrothermal alteration of fresh rhyolite and weakly altered dacitic tuff with artificial seawater at 300 °C and 1 bar for 5 and 29 days and found changes in the fluid composition during smectite formation [18].

In the middle to southern Okinawa Trough in the East China Sea, several ABA hydrothermal fields have been found (e.g., [3,4,19]). Previous observations of natural fluid chemistry suggested that, in the hydrothermal fields in the trough, the fluid composition is controlled at least in part by reactions with intermediate-to-felsic rocks [20–23]. Some of the hydrothermal systems in the Okinawa Trough are associated with subseafloor massive sulfide (SMS) deposits, a modern analog of the Kuroko-type volcanogenic massive sulfide (VMS) deposit [24]. Nozaki et al. (2021) recently pointed out that the subseafloor replacement of pumice by sulfide minerals is a key process of the SMS deposit formation in the trough [25]. According to their scenario, pyrite framboids in close association with amorphous material derived from altered glass in pumice are replaced later with other sulfides from large SMS deposits via pumice replacement mineralization beneath the seafloor. Their study implies that the behavior of volcanic glass in the hydrothermal alteration of intermediate-to-felsic rocks is an important controlling factor not only for the fluid composition but also for the SMS deposit formation in the Okinawa Trough. However,

no previous experimental study of intermediate-to-felsic rocks focused particularly on the behavior of silica in the hydrothermal water–rock reactions.

In this study, we experimentally analyzed fresh rhyolite and andesite rocks from the middle and southern Okinawa Trough, respectively, where active hydrothermal vents are observed. We examined their hydrothermal alteration processes by using a steel-alloy autoclave at 325 °C and 300 bar, the estimated condition at the reaction zone in the systems in the trough. We monitored the fluid composition during the experiments and observed the microtexture of volcanic glass in the reaction products of the analyzed rocks. Based on these results, we discussed the behavior of silica during the hydrothermal alteration of the rocks and its contribution to the chemical composition of the fluids. We also infer a potential role of glass alteration in the SMS deposit formation in the middle to southern Okinawa Trough.

2. Geological Background and Analyzed Materials

The Okinawa Trough is a back-arc basin located along the eastern margin of the Eurasian continent, extending for >1200 km from the Japanese island to Taiwan along the Ryukyu Arc [26]. Previous studies identified three phases of extension from the middle-to-late Pleistocene to the present in the Okinawa Trough in the rifting stage of back-arc basin formation [26–28]. Several active hydrothermal sites have been found in the Okinawa Trough mostly at a water depth of ca. 1000 to 1500 m and massive sulfide and sulfate mineralization is recognized in some hydrothermal fields [3,4,22,29]. The SMS deposits in the Okinawa Trough have been generally considered to be a modern analog of the Kuroko-type VMS deposits on land [24–26].

The fresh rhyolite sample analyzed in the present experiment was collected from the Iheya graben in the middle Okinawa Trough. The unaltered rhyolite sample (CB6-20DR3-1) was collected by dredging from the northern fringe of the Natsushima 84-1 Knoll (27°34.57' N, 127°08.37' E, 1600 m water depth) in the R/V Hakuho-maru KH-87-2 cruise in May 1987 during the “Corona Borealis (CB)” expedition [30,31]. The analyzed rhyolite is light-gray-colored with some several mm sized elongated void parts (Figure 1a). Flow structures are developed in the rock. Under the microscope, the rhyolite with a slightly porphyritic texture contains subhedral-to-euhedral phenocrysts of plagioclase, amphibole, clinopyroxene, and minor Fe-Ti oxides (Figure 1b,c). Plagioclase phenocrysts (<3 mm) are largely columnar-shaped. The size of mostly elongated amphibole phenocryst ranges from 100 to 1000 µm. The groundmass of the rhyolite rock is composed mainly of microlites of elongated plagioclase (<65 µm) aligned along the flow structures and of glass.

The fresh andesite sample was collected from the Hatoma Knoll hydrothermal field in the southern Okinawa Trough. The Hatoma Knoll hydrothermal field is located in the summit crater (~600 m in diameter) of the Hatoma Knoll in the southern Okinawa Trough at the water depth of ~1500 m [22]. Hydrothermal activity (<325 °C) and sulfide–sulfate mineralization is recognized in several sites within the crater, including a dacite cone with large active chimneys at the center of the crater. The fresh unaltered andesite sample (HPD#1621-R09) was collected from the northeastern fringe of the crater (24°51.5787' N, 123°50.7177' E, 1404 m water depth) during the R/V Kaiyo KY14-02 cruise in February 2014 by using a ROV Hyper Dolphin 3000 (Figure 1d). The analyzed andesite sample shows a light gray color with some several mm sized elongated void parts (Figure 1e). Flow structures are developed in the rock. Under the microscope, the andesite with a porphyritic texture contains subhedral-to-euhedral phenocrysts of plagioclase (<0.6 mm) and clinopyroxene (<1.2 mm) (Figure 1f,g). Plagioclase crystals are largely columnar and sometimes form aggregates. Zonal structures are rarely observed in the plagioclase crystals. Some clinopyroxene crystals also form aggregates. The groundmass of the andesite is composed of elongated plagioclase and clinopyroxene (<60 µm), mainly aligned along the flow structures in the rock. Also, euhedral magnetite (~10 µm in diameter) and brown volcanic glass are frequently observed (Figure 1h).

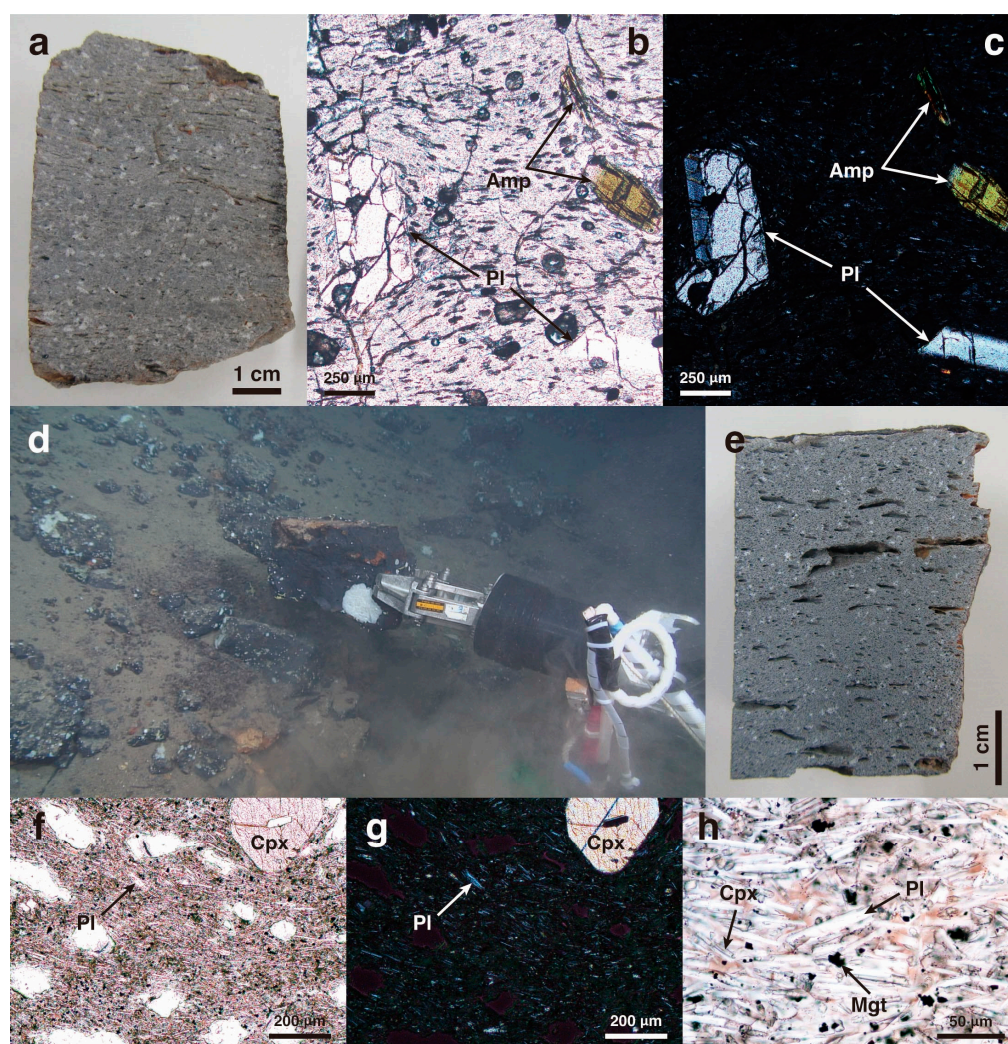


Figure 1. Analyzed rock samples. (a–c) Polished slab (a) and photomicrographs (b,c) of the analyzed rhyolite. (b) (opened nicols) and (c) (crossed nicols) show the same field of view. Pl: plagioclase; Amp: amphibole. (d–h) Sampling photo by ROV Hyper Dolphin 3000 (d), polished slab (e), and photomicrographs (f–h) of the analyzed andesite. (f) (opened nicols) and (g) (crossed nicols) show the same field of view. Cpx: clinopyroxene; Mgt: magnetite. In (h), elongated plagioclase and clinopyroxene crystals with flow texture and volcanic glass (brown areas) are observed.

3. Experimental System and Sample Analyses

The hydrothermal reaction was simulated in a steel-alloy autoclave at JAMSTEC (Figure 2; e.g., [10,11,32]). The reaction cell consisted of a flexible gold tube with a Ti head. The rock sample was powdered (<90 μm in diameter) by using an agate ball mill and a sieve. The rock powder was cleaned with ultrapure water and acetone several times and was dried at 50 $^{\circ}\text{C}$. To prepare the artificial seawater, NaCl reagent was dissolved in ultrapure water to 500 mM. The powdered rock sample was reacted with the artificial seawater in the reaction cell at 325 $^{\circ}\text{C}$ and 300 bar—the estimated seafloor reaction zone condition where the hydrothermal fluid reacts with surrounding rocks in the Okinawa Trough (~1000 mbsf; e.g., [22]). The initial water/rock ratio was adjusted to be ~4 (~12 g of rock powder and ~50 g of artificial seawater) as the water/rock ratio in seafloor hydrothermal systems is considered to be generally <5 [33]. During the experiments, the reacted fluid (~4 g) in the reaction cell was obtained several times through a gold-lined sampling tube.

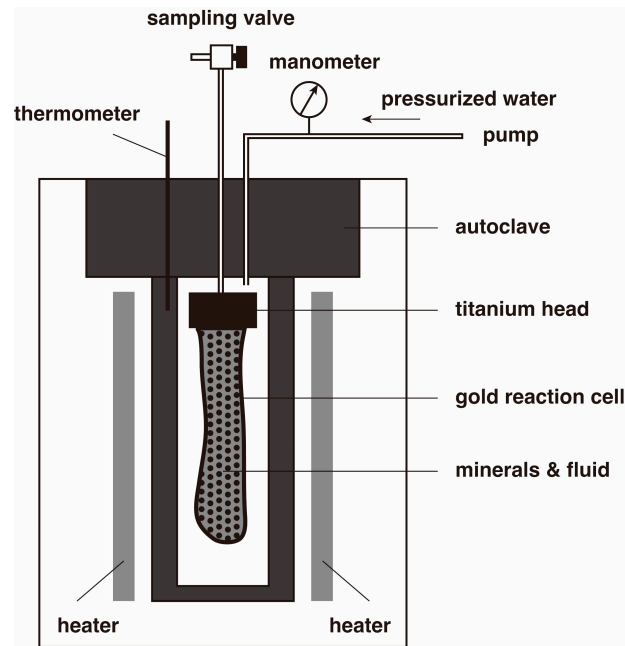


Figure 2. Schematic diagram of the hydrothermal experimental apparatus.

3.1. Liquid-Phase Analyses

For cation analyses, 0.2 mL of fluid was sampled in a vial, and HNO_3 was added to avoid mineral precipitation. For anion analyses, 0.2 mL of fluid was collected, and NaOH was added. The concentrations of Cl, Na, and K were analyzed with ion chromatography (Dionex ICS-1600/2100, Thermo Fisher Scientific, Waltham, MA, USA), while those of Al, Ca, Mg, Fe, Mn, and Si were analyzed with inductively coupled plasma optical emission spectrometry (ICP-OES) (SPS5510, Seiko Instruments Inc., Chiba, Japan) at JAMSTEC. The analytical precision (1RSD; $n = 3$) of replicate measurements was $<2\%$ for Cl, Na, and K and $<5\text{--}10\%$ for the other elements depending on their concentrations. The detection limit for each element in the ion chromatography and ICP-OES measurements was ≤ 0.01 mg/L.

For pH analysis, 1.0 mL of fluid was collected in a vial, and the pH was measured with a pH meter (LAQUAtwin, HORIBA Ltd., Kyoto, Japan) at room temperature under atmospheric conditions. The estimated precision of pH measurement was ± 0.1 . For H_2 analysis, 0.5 mL of fluid was introduced to an Ar-purged vial. The vial was left for >30 min to reach equilibrium at room temperature. The H_2 concentration in the vial headspace was measured with gas chromatography (GC-2014, SHIMADZU Corp., Kyoto, Japan) at JAMSTEC. The detection limit for H_2 in the gas chromatography analyses was <1.0 $\mu\text{mol/kg}$. For H_2S analysis, 1.5 mL of fluid was introduced to an Ar-purged vial. Then, 1N HCl was added to the fluid immediately after the sampling to decrease the pH of the fluid and to convert HS^- and S^{2-} to H_2S in equilibrium. The H_2S concentration in the fluid was analyzed with a standard methylene blue method using NANOCOLOR Standard Test Sulphide (MACHEREY-NAGEL, Düren, Germany) and a UV-visible spectrophotometer (UV-1600, SHIMADZU Corp., Kyoto, Japan). The detection limit for H_2S in the UV-visible spectrophotometer analyses was <0.5 $\mu\text{mol/kg}$. The analytical precision (1RSD) of replicate measurements was $<5\%$ and $<4\%$ for the H_2 and H_2S concentrations, respectively.

3.2. Solid-Phase Analyses

The whole-rock composition of 10 major elements (Si, Ti, Al, Fe, Mn, Mg, Ca, Na, K, and P) of the starting rhyolite and andesite sample was analyzed with X-ray Fluorescence (XRF) (Simultix 12, Rigaku Corp., Tokyo, Japan) analysis at JAMSTEC (Table 1). The mineral composition of the rock samples before and after the hydrothermal experiments was analyzed using a wavelength-dispersive-type Electron Probe Micro-Analyzer (EPMA) (JXA-8500F, JEOL Ltd., Tokyo, Japan) and a desktop X-ray diffractometer (XRD)

(MiniFlex II, Rigaku Corp., Tokyo, Japan) at JAMSTEC. The EPMA analyses were conducted at 15 kV of accelerating voltage, 12 nA of specimen current, and 1 and 5 μm of probe diameter. The XRD analyses were conducted at 30 kV and 15 mA using $\text{CuK}\alpha$ radiation. Dried sample powder was mounted on plastic holders ($\phi = 20$ mm, depth = 0.5 mm), and the oriented samples were scanned over an interval of 3° – 90° (2θ).

Table 1. Composition of the solid starting materials (wt.%). LOI: loss on ignition.

	Rhyolite	Andesite
SiO_2	73.8	61.9
TiO_2	0.3	0.9
Al_2O_3	13.9	15.2
Fe_2O_3	2.1	9.7
MnO	0.1	0.2
MgO	0.3	1.7
CaO	1.8	6.1
Na_2O	4.5	3.4
K_2O	2.9	0.9
P_2O_5	0.1	0.2
Total	99.6	100.0
LOI	2.0	0.0

4. Results

Figure 3 and Table 2 show the time variation in the concentration of selected elements and in that of the dissolved gas species and pH, respectively, in the reacted fluids. The Cl concentration in the fluids was rather constant (~ 500 mmol/kg) during the experiments. The Na concentration in the fluids gradually decreased from ~ 500 to ~ 460 – 470 mmol/kg during the experiments. The K concentration abruptly increased up to ~ 40 mmol/kg within 24 h and was rather constant in the rhyolite experiment, while the concentration increased up to ~ 20 mmol/kg within 24 h and gradually increased to ~ 35 mmol/kg in the andesite experiment. The Si concentration in the fluid also increased abruptly and then remained considerably high, ~ 30 mmol/kg and ~ 20 mmol/kg in the rhyolite and andesite experiments, respectively. The Ca concentration rose within 24 h and then gradually increased in the experiments. The Fe, Mn, and Mg concentrations remained consistently low (<10 $\mu\text{mol/kg}$) during both of the experiments. The pH value decreased from 7.0 to 4.5 in the rhyolite experiment, while the value decreased from 7.0 to 4.1 and then gradually increased to 5.5 in the andesite experiment. The H_2 and H_2S concentrations in the fluids generally increased during the experiments.

Figure 4 shows the powder XRD patterns of the starting materials and reaction products of the experiments. The XRD patterns are generally consistent with the microscopic descriptions of the analyzed volcanic rocks (Figure 1). The peaks of andesine are clearly observed both in the starting material and reaction product of the analyzed rhyolite. On the other hand, the peaks of plagioclase and clinopyroxene are observed both in the starting material and reaction product of the andesite. No significant change in the whole XRD pattern was recognized in both the rhyolite and andesite experiments.

The SEM observation of analyzed rhyolite and andesite shows that volcanic glass was substantially dissolved during the hydrothermal experiment (Figure 5). The surface of starting material grains is rather smooth and dense, whereas the surface of the reaction product grains is rough and porous. No clear evidence of substantial dissolution of other minerals was recognized under the microscope, and those minerals appear to be “etched” on the rough surface of reaction products (Figure 5b,d,f). Those textures demonstrate the preferential dissolution of volcanic glass in rhyolite via hydrothermal alteration. However, the rim of the reaction product grains of rhyolite is rather dense, possibly owing to the precipitation of amorphous silica from the fluid (Figure 6). The precipitation of nanoparticles was also observed within some pores in the reaction products. The nanoparticles are possibly amorphous silica although they are too small to be analyzed with EPMA spot

analysis. The precipitation of nanoparticles was clearly recognized at the rim of the reaction product grains of andesite (Figure 6c). The nanoparticles are also possibly amorphous silica though they are too small to be analyzed with EPMA.

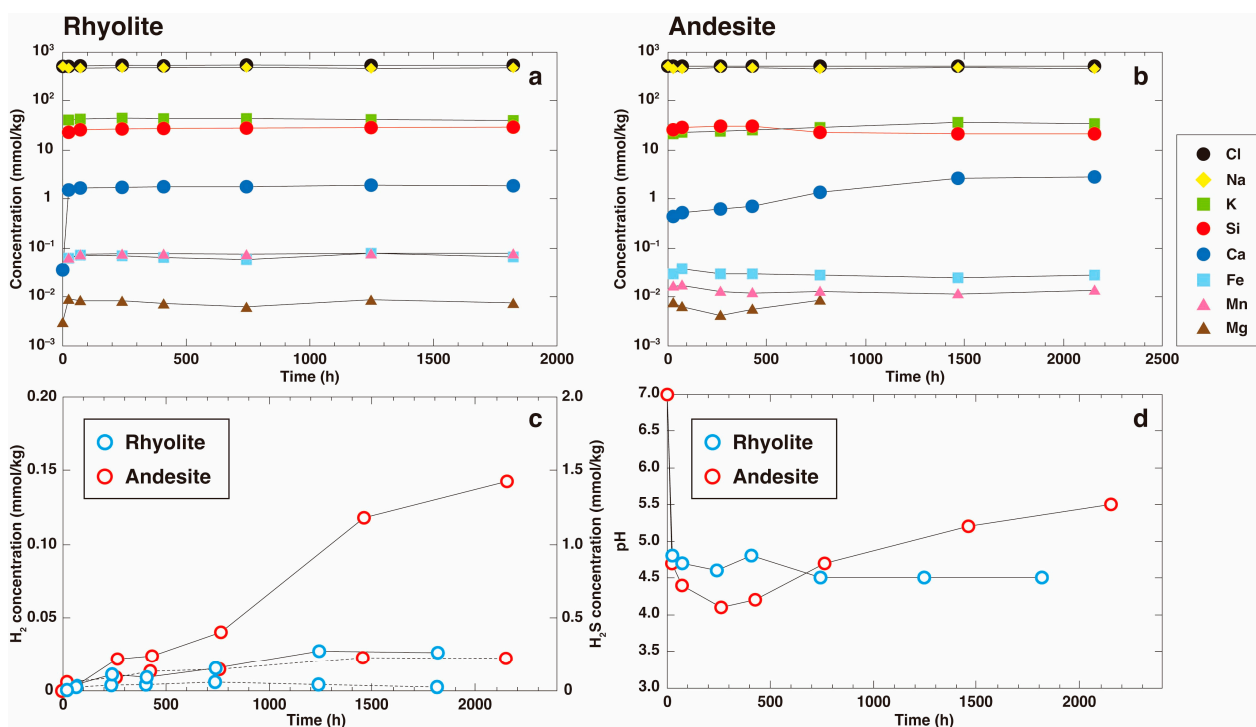


Figure 3. Time variation in fluid composition in the hydrothermal experiments. (a,b) The concentration of selected elements in rhyolite (a) and andesite (b) experiments. (c) The concentration of dissolved H₂ and H₂S (solid and dashed lines, respectively). (d) pH.

Table 2. Fluid composition in the hydrothermal experiments (mmol/kg).

Rhyolite											
Time (h)	Cl	Na	K	Mg	Ca	Si	Fe	Mn	H ₂	H ₂ S	pH
0	506	503	n.d.	0.00	0.00	n.d.	n.d.	n.d.	0.00	0.00	7.0
24	501	461	40.4	0.01	1.49	22.6	0.06	0.06	0.00	0.00	4.8
70	505	453	41.9	0.01	1.64	25.0	0.07	0.07	0.00	0.00	4.7
240	524	470	43.9	0.01	1.73	26.5	0.07	0.07	0.01	0.04	4.6
408	515	462	42.6	0.01	1.76	26.8	0.06	0.07	0.01	0.04	4.8
744	532	477	42.8	0.01	1.75	27.7	0.06	0.07	0.02	0.06	4.5
1248	519	455	40.7	0.00	1.85	28.1	0.08	0.08	0.03	0.04	4.5
1824	517	470	39.7	0.00	1.82	29.0	0.07	0.07	0.03	0.02	4.5
Andesite											
Time (h)	Cl	Na	K	Mg	Ca	Si	Fe	Mn	H ₂	H ₂ S	pH
0	504	499	n.d.	n.d.	n.d.	0.00	n.d.	n.d.	n.d.	n.d.	7.0
24	494	459	21.9	0.01	0.43	25.3	0.03	0.02	0.00	0.06	4.7
71	502	460	22.6	0.01	0.52	28.5	0.04	0.02	0.01	n.d.	4.4
262	499	470	24.2	0.00	0.61	30.0	0.03	0.01	0.02	0.09	4.1
429	506	480	25.0	0.01	0.71	29.7	0.03	0.01	0.03	0.13	4.2
766	502	458	29.5	0.01	1.34	22.3	0.03	0.01	0.04	0.14	4.7
1463	512	464	35.5	n.d.	2.60	21.9	0.02	0.01	0.12	0.22	5.2
2158	505	457	34.2	n.d.	2.78	21.7	0.03	0.01	0.14	0.22	5.5

n.d.: not detected.

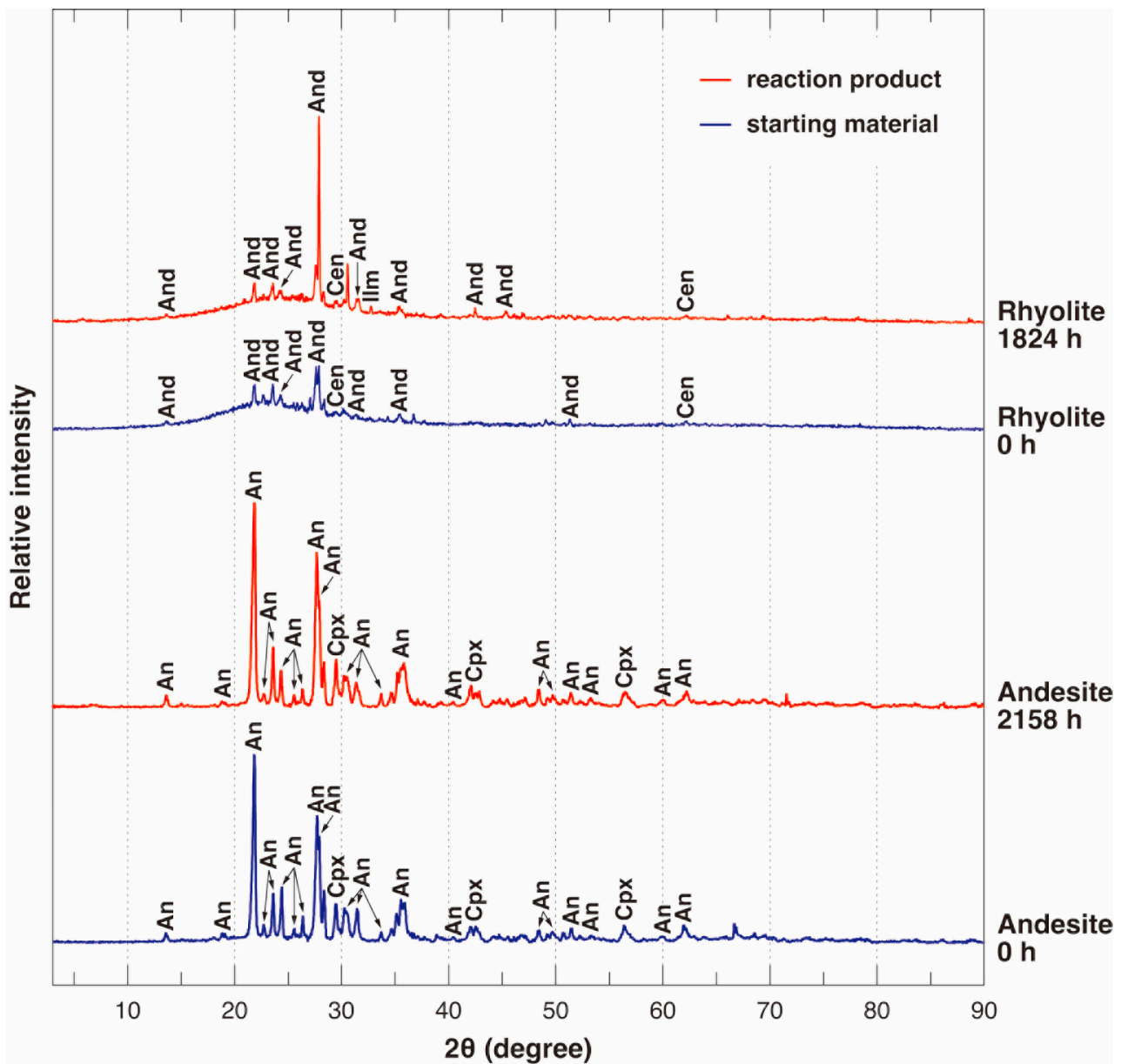


Figure 4. Powder XRD patterns (CuK α) of the analyzed rhyolite and andesite. And: andesine; Cen: clinoenstatite; Ilm: ilmenite; An: anorthite; Cpx: clinopyroxene.

Figure 7a,b show the EPMA results of rhyolite. The plagioclase both in the starting material and reaction product is mainly andesine with finer oligoclase grains. No orthoclase was recognized. The analyzed clinopyroxene both in the starting material and reaction product is mostly (clino)enstatite although minor augite and pigeonite were observed in the starting material and reaction product, respectively.

The EPMA results show that the volcanic glass is relatively enriched in K (2.5 mol% on average) compared to in other mineral grains (Table 3). During the hydrothermal experiment, K was leached into the fluid and became depleted in the solid glass (Figure 8). The EPMA results of the glass also show that the rim of the reaction product grains (filled circles in Figure 8) is relatively enriched in Si compared to the internal parts. We interpret that this is due to the precipitation of amorphous silica at the rim during the experiment. This interpretation is consistent with the observed contrast between the dense rim and porous internal part of the reaction product grains (Figures 5 and 6).

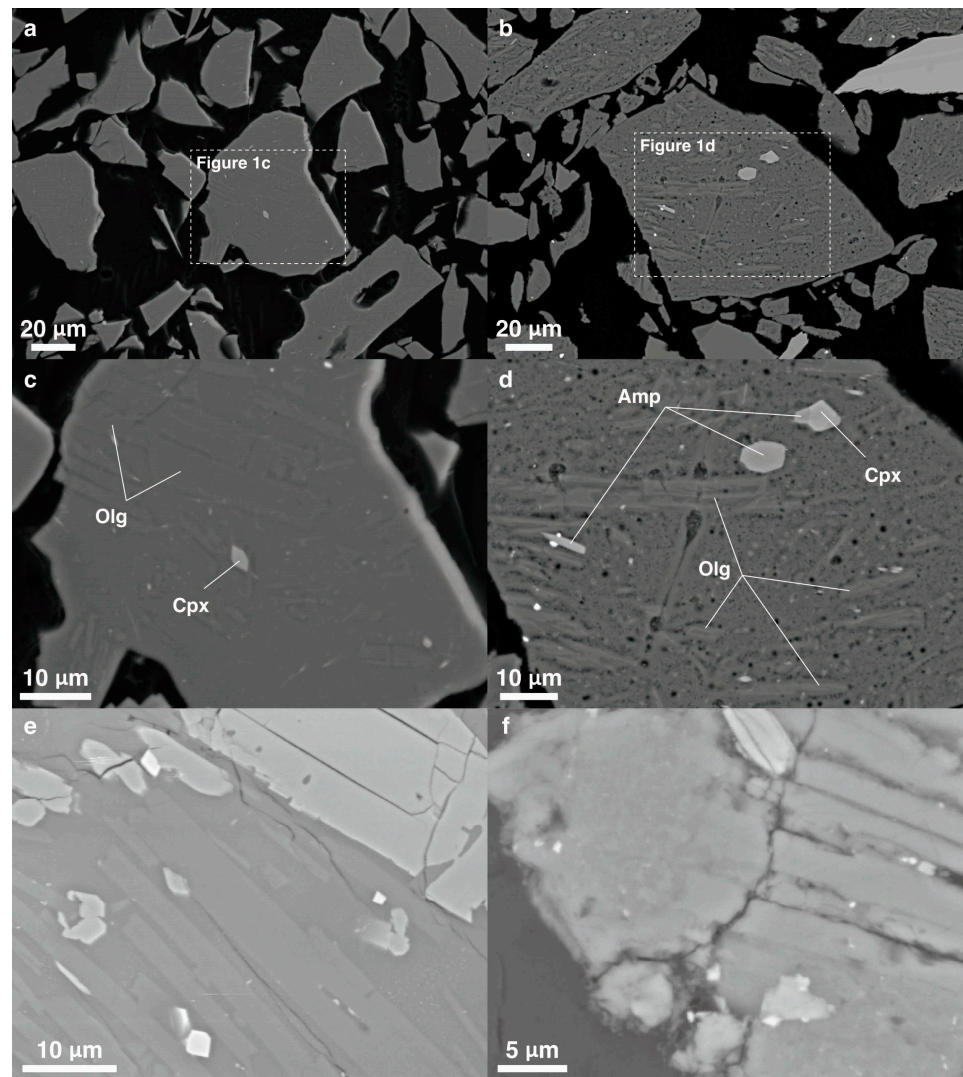


Figure 5. Backscattered electron (BSE) images of analyzed fine grains of rhyolite (a–d) and andesite (e,f), showing substantial and preferential glass dissolution. (a,c,e) Starting materials. (b,d,f) Reaction products. Note the clear contrast between the smooth surface of starting material and the rough and porous surface of reaction product, which shows the preferential dissolution of volcanic glass via hydrothermal alteration. Olg: oligoclase; Cpx: clinopyroxene; Amp: amphibole.

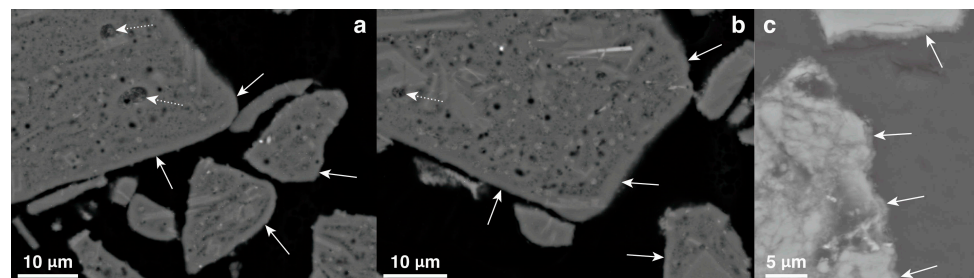


Figure 6. BSE images of the rim of reaction product grains. (a,b) Rhyolite. Although the internal part of the grains is porous, the 2–3 μm thick rim of the grains is rather dense (solid arrows), possibly due to the precipitation of amorphous silica. The precipitation of nanoparticles (possibly amorphous silica) is also observed within some pores (dashed arrows). Also see Figure 8. (c) Andesite. The precipitation of nanoparticles (possibly amorphous silica) is commonly observed at the rim of grains (arrows). Also see Figure 5f.

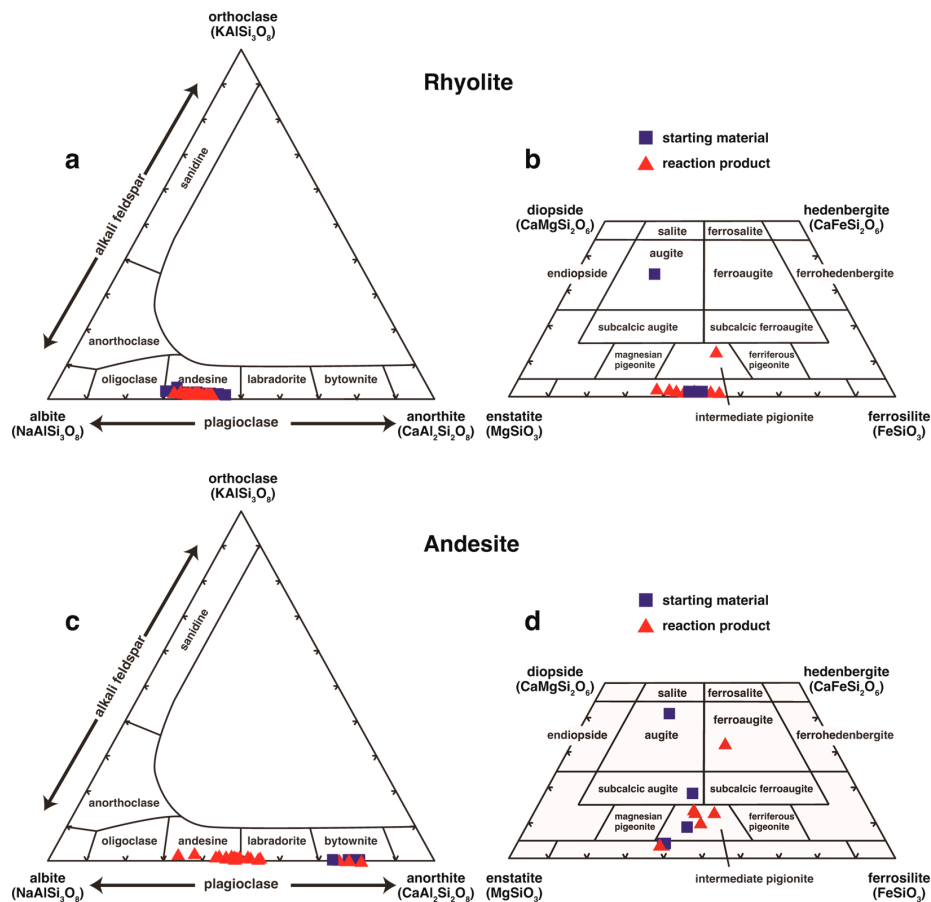


Figure 7. EPMA results of the analyzed rhyolite (a,b) and andesite (c,d). Plagioclase (a,c) and pyroxene (b,d) compositions of starting materials (blue square) and reaction products (red triangle) of the experiment in the feldspar and pyroxene diagrams, respectively. Orthoclase grains in rhyolite are too small for spot analysis and are not shown.

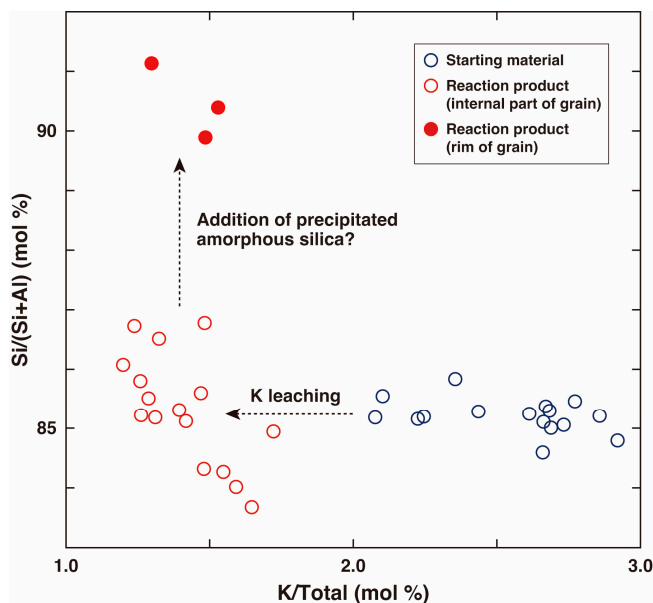


Figure 8. EPMA results of the glass in the rhyolite. The K concentration in the glass decreased during hydrothermal alteration via K leaching into the fluid. Also see Table 2. Note that the glass at the rim of the reaction product grains is depleted in Al (filled circle). This is possibly due to the precipitation of amorphous silica at the rim from the fluid. Also see Figure 6.

Table 3. EPMA results of the glass in the rhyolite (mol%, except for Total wt.%).

Starting Material	Si	Ti	Al	Fe	Mg	Mn	Ca	Na	K	Cr	P	Ni	S	Total wt.%
Glass	77.0	0.1	14.0	0.9	0.1	0.0	0.9	4.3	2.7	0.0	0.0	0.0	0.0	99.5
Glass	76.8	0.1	13.8	1.0	0.0	0.0	0.9	4.5	2.9	0.0	0.0	0.0	0.0	92.2
Glass	77.4	0.1	13.7	0.9	0.0	0.0	0.9	4.1	2.7	0.0	0.0	0.0	0.0	95.2
Glass	77.3	0.1	13.6	0.9	0.1	0.0	0.9	4.3	2.7	0.0	0.0	0.0	0.0	94.8
Glass	77.5	0.1	13.6	0.9	0.1	0.0	0.8	4.3	2.7	0.0	0.0	0.0	0.0	94.7
Glass	78.7	0.1	13.7	0.9	0.0	0.0	0.8	3.5	2.2	0.0	0.0	0.0	0.0	95.1
Glass	78.4	0.1	13.6	0.9	0.2	0.0	0.8	3.9	2.1	0.0	0.0	0.0	0.0	95.7
Glass	78.3	0.2	13.6	0.9	0.0	0.1	0.8	3.8	2.2	0.0	0.0	0.0	0.0	97.4
Glass	77.6	0.1	13.5	0.8	0.1	0.1	0.9	4.1	2.9	0.0	0.0	0.0	0.0	98.1
Glass	77.7	0.1	13.5	0.9	0.1	0.0	0.9	4.2	2.6	0.0	0.0	0.0	0.0	95.1
Glass	77.9	0.1	13.4	0.9	0.1	0.1	0.9	4.1	2.4	0.1	0.0	0.0	0.0	97.1
Glass	77.5	0.1	13.4	1.1	0.2	0.1	0.8	4.1	2.7	0.0	0.0	0.0	0.0	95.3
Glass	77.6	0.1	13.3	0.9	0.1	0.0	0.9	4.3	2.7	0.1	0.0	0.0	0.0	95.7
Glass	78.2	0.1	13.3	0.8	0.0	0.0	0.8	4.0	2.8	0.0	0.0	0.0	0.0	95.4
Glass	78.3	0.1	13.2	0.8	0.1	0.1	0.8	4.4	2.1	0.0	0.0	0.1	0.0	97.7
Glass	79.0	0.1	13.0	0.9	0.1	0.0	0.7	3.8	2.4	0.0	0.0	0.0	0.0	96.9
Andesine (av.; n = 16)	54.2	0.0	26.2	0.2	0.0	0.0	7.1	11.9	0.3	0.0	0.0	0.0	0.0	100.4
Pyroxene (av.; n = 7)	50.0	0.1	0.5	20.6	24.1	0.9	3.7	0.1	0.0	0.0	0.0	0.0	0.0	100.4
Reaction product	Si	Ti	Al	Fe	Mg	Mn	Ca	Na	K	Cr	P	Ni	S	Total wt.%
Glass (int.)	77.9	0.0	15.2	0.8	0.1	0.1	0.8	3.3	1.6	0.1	0.0	0.0	0.0	88.1
Glass (int.)	77.7	0.1	14.8	1.1	0.3	0.0	0.7	3.5	1.6	0.0	0.0	0.1	0.0	58.0
Glass (int.)	78.3	0.1	14.6	1.1	0.1	0.0	0.8	3.2	1.5	0.0	0.0	0.0	0.0	91.2
Glass (int.)	79.4	0.1	14.8	1.2	0.1	0.0	0.8	2.0	1.5	0.0	0.0	0.0	0.0	90.4
Glass (int.)	79.6	0.1	14.1	0.5	0.1	0.0	0.8	3.0	1.7	0.0	0.0	0.0	0.0	63.9
Glass (int.)	78.4	0.1	13.7	1.1	0.2	0.0	0.7	4.4	1.4	0.0	0.0	0.0	0.0	92.5
Glass (int.)	79.3	0.1	13.8	0.8	0.0	0.1	0.7	3.8	1.3	0.0	0.0	0.0	0.0	95.2
Glass (int.)	80.6	0.1	14.0	0.6	0.0	0.0	0.7	2.7	1.3	0.0	0.0	0.0	0.1	93.2
Glass (int.)	79.7	0.1	13.7	1.0	0.1	0.1	0.7	3.2	1.4	0.0	0.0	0.0	0.0	94.8
Glass (int.)	79.9	0.1	13.5	1.2	0.1	0.0	0.7	3.1	1.3	0.0	0.0	0.0	0.0	92.4
Glass (int.)	80.7	0.1	13.6	0.7	0.1	0.0	0.7	2.7	1.5	0.0	0.0	0.0	0.0	95.8
Glass (int.)	81.5	0.1	13.5	0.7	0.0	0.0	0.7	2.3	1.3	0.0	0.0	0.0	0.0	92.9
Glass (int.)	81.9	0.1	13.3	0.5	0.1	0.0	0.6	2.3	1.2	0.0	0.0	0.0	0.0	82.3
Glass (int.)	82.1	0.1	12.8	0.7	0.1	0.0	0.8	2.0	1.3	0.0	0.0	0.0	0.0	84.0
Glass (int.)	81.7	0.1	12.5	0.7	0.1	0.1	0.7	2.9	1.2	0.0	0.0	0.0	0.0	91.8
Glass (int.)	82.3	0.2	12.5	0.6	0.1	0.1	0.6	2.0	1.5	0.0	0.0	0.0	0.0	92.2
Glass (rim)	85.5	0.0	9.6	0.2	0.0	0.0	0.5	2.6	1.5	0.0	0.0	0.0	0.0	71.2
Glass (rim)	84.9	0.1	9.0	0.7	0.1	0.1	0.8	2.8	1.5	0.0	0.0	0.0	0.0	70.3
Glass (rim)	87.2	0.0	8.5	0.1	0.0	0.0	0.4	2.4	1.3	0.0	0.0	0.1	0.0	85.9
Andesine (av.; n = 33)	54.0	0.0	26.4	0.2	0.0	0.0	7.2	11.7	0.3	0.0	0.0	0.0	0.0	99.7
Pyroxene (av.; n = 14)	49.9	0.1	0.8	21.8	24.8	0.9	1.4	0.1	0.0	0.0	0.0	0.0	0.0	100.5

av.: average; rim: rim of grain; int.: internal part of grain.

The EPMA results of rhyolite illustrate no substantial change in the mineral composition of plagioclase and of clinopyroxene via hydrothermal alteration during the experiment (Figure 7). This is consistent with the powder XRD patterns (Figure 4) and with the SEM observation showing that only the volcanic glass was substantially dissolved during the experiment (Figure 5).

Figure 7c,d show the EPMA results of andesite sample. Plagioclase in the starting material is mainly anorthite, and no orthoclase was recognized. In contrast, plagioclase in the reaction products is classified mainly into albite, although some anorthite minerals

still remain. The difference in the mineral composition of feldspar between the starting material and reaction product suggests some albitization of anorthite via hydrothermal alteration [34]. The clinopyroxene both in the starting material and reaction product is classified mostly into augite, pigeonite, and (clino)enstatite. No substantial change was observed in the mineral composition of clinopyroxene during the experiment.

5. Discussion

5.1. Substantially Si-Enriched Fluids

The hydrothermal fluids reacted with the analyzed rhyolite and andesite in the present experiments are characterized by the substantially high Si concentration, up to 30 mM (Figure 3). The Si concentration in the fluid, which is in equilibrium with quartz at 325 °C and 300 bar, is estimated to be ~14 mM [35]. Therefore, the high Si concentration in the present fluids cannot be explained by the equilibrium with quartz. Alternatively, hydrothermal experiments and numerical thermodynamic calculations indicated that the Si concentration in the fluid, which is in equilibrium with amorphous silica, is much higher, ~30 mM, at 325 °C (Figure 9) [36]. We interpret that, in the present experiments, the substantial dissolution of volcanic glass in the analyzed rocks increased the Si concentration in the fluids. We further interpret that the high Si concentration in the fluids (up to 30 mM) was maintained during the experiments by buffering by amorphous silica, precipitated from the fluids as a precursor of hydrothermal quartz. Indeed, as described in Section 4, the preferential dissolution of volcanic glass via hydrothermal alteration in the analyzed volcanic rocks is directly supported by the results of SEM observation (Figure 5).

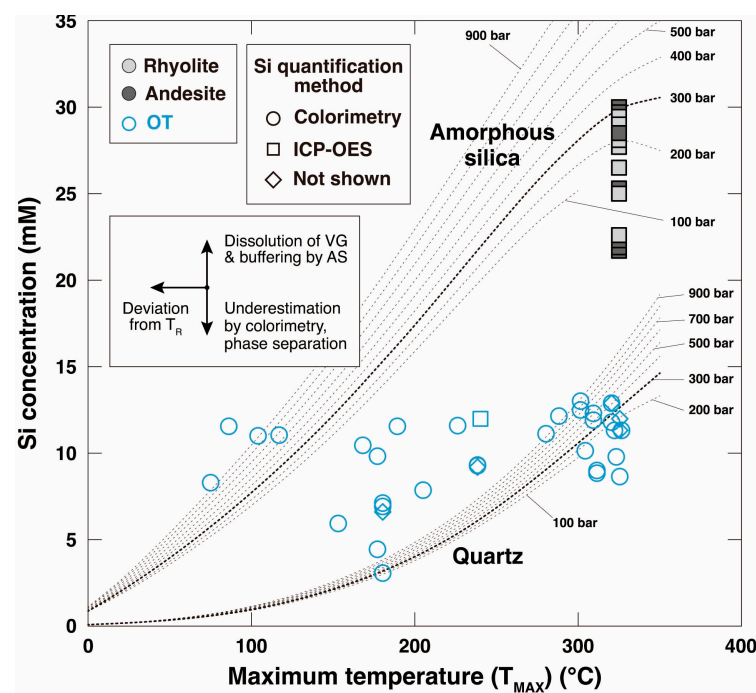


Figure 9. The maximum temperature (T_{MAX}) of the observed fluid and the Si concentration in estimated endmember fluids in the hydrothermal fields in the Okinawa Trough (OT), with the solubility curve of quartz and of amorphous silica at 100–900 bar (dashed). Potential biases/effects on each point are shown in the inset. T_R : temperature at the reaction zone; VG: volcanic glass; AS: amorphous silica. The present experimental results are also shown for comparison. The Si concentration in most fluids (especially with $T_{MAX} < 250$ °C) is apparently too high to be explained by the equilibrium with quartz. References for the compilation are listed in the Supplementary Information (Table S1, [37–51]).

In addition to the glass dissolution, the precipitation of amorphous silica from the fluids in the present experiments is also supported by the results of SEM observation

(Figure 6). As discussed above, the internal part of the reaction product grains is porous due to the preferential dissolution of volcanic glass via hydrothermal alteration (Figure 5). However, the SEM observations also reveal that the 2–3 μm thick rim of the reaction product grains of rhyolite is rather dense. We infer that the dense rim of the rhyolite grains is attributed to the precipitation of amorphous silica nanoparticles from the fluid during the experiment. The precipitation of nanoparticles is also observed within some pores in the reaction products of rhyolite (dashed arrows in Figure 6). Although they are too small to be analyzed with EPMA spot analysis, we infer that these nanoparticles are also amorphous silica. The precipitation of amorphous silica at the rim of the reaction product grains is further supported by the EPMA results of the glass in rhyolite (Figure 8). The results show that the glass at the rim of the reaction product grains is relatively enriched in Si compared to in their internal part. This can be attributed to the addition of precipitated amorphous silica at the rim.

The microtexture of andesite grains is generally similar to that of rhyolite grains (Figures 5 and 6). A contrast between the smooth surface of the starting material and the rough surface of the reaction product was observed (Figure 5e,f), suggesting the preferential dissolution of volcanic glass during the hydrothermal experiment. Moreover, the precipitation of nanoparticles at the rim of the reaction product grains is commonly observed in the andesite experiment (Figure 6c). Again, the nanoparticles are too small to be analyzed with EPMA, but we infer that these nanoparticles are amorphous silica. The present texture is somewhat similar to the amorphous Si-rich phase (with saponite) encrusting the host phases via the hydrothermal alteration of synthetic chondrite [52].

We infer that the amorphous silica precipitated from the present fluids as a precursor of hydrothermal quartz. In general, amorphous silica (opal-A) is metastable under high-temperature and -pressure conditions and would be transformed into quartz at 325 $^{\circ}\text{C}$ and 300 bar [35]. In this case, the fluids could have been in equilibrium with the generated quartz in the reaction cell. However, the substantially high Si concentration in the fluids suggests that, in the present experiments, the amorphous silica was not replaced with secondary quartz and the fluids did not reach equilibrium with quartz. This interpretation is consistent with the results of the SEM observations and of the EPMA and XRD analyses, in which no evidence of quartz generation was recognized in the reaction products (Figures 4 and 5).

The substantially high Si concentration in the fluids (up to 30 mM) in the present experiments is consistent with the previous experimental results in Shiraki et al. (1987) [16]. Although their experiments were conducted at 300 $^{\circ}\text{C}$ and 1000 bar, the Si concentration in the fluid (measured with silico-molybdc colorimetry) was up to ~ 33 mM in the rhyolite experiment and ~ 23 mM in the andesite experiment. These values are significantly higher than the Si concentration in the fluid which is in equilibrium with quartz at 300 $^{\circ}\text{C}$ and 1000 bar (~ 15.5 mM; [35]). The experimental fluids were not in equilibrium with quartz but were likely buffered by amorphous silica precipitated from the fluids. It is worthy to note that Shiraki et al. also suggested that, in their andesite experiment, the steady state in the reaction cell was not attained over 7000 h [16]. Although the steady state was thought to be attained quickly (<48 h) in their rhyolite experiment and the cause of this substantial difference between the rhyolite and andesite experiments was uncertain, their observation is consistent with the results of our experiments indicating that, at 325 $^{\circ}\text{C}$ and 300 bar, the fluids did not reach equilibrium with quartz during the experiments over 1800 h.

The reason for the disequilibrium in the previous and present experiments remains uncertain. For example, the nanoparticles of amorphous silica precipitated on the surface of rock grains may have encrusted the grains and have delayed the additional chemical reaction between the rock grains and fluid. Potentially related to this, the grain size of the rock powder used in the hydrothermal experiments might have also been a key factor in the time duration to reach equilibrium between the solid and liquid phases. Shiraki et al. used rock powder of <75 μm in diameter for the rhyolite experiment and interpreted that the steady state was attained within 48 h. On the other hand, they used rock powder of 75–150 μm in diameter for the andesite experiment and concluded that the steady state was

not attained over 7000 h. In the present rhyolite and andesite experiments, we used rock powder of $<90\ \mu\text{m}$ in diameter (Section 3). While details are still unknown, the difference in the grain size of the rock powder, and consequently in the total surface area between the solid and liquid phases in the reaction cell, may have influenced the time required to reach equilibrium in both the previous and present experiments.

Overall, the Si concentration in the experimental fluid was not substantially different between the rhyolite and andesite experiments. However, the Si concentration monotonously increased during the rhyolite experiment. In contrast, in the andesite experiment, the concentration peaked at 30.0 mmol/kg after 262 h and then gradually decreased to 21.7 mmol/kg by 2158 h. As discussed above, the fluids did not reach equilibrium with quartz both in the rhyolite and andesite experiments. Moreover, no evidence of quartz generation was recognized in the reaction products (Figures 4 and 5). Nonetheless, the decrease in the Si concentration in the andesite experiment implies that the fluid might have been moving towards equilibrium with quartz.

5.2. Behavior of Elements Other than Si in the Fluids

The EPMA results of rhyolite show that K is relatively enriched in volcanic glass (ca. 2.5 mol% on average) compared to in other mineral grains (less than 0.5 mol% on average; Table 3) in the starting materials. This fact supports the substantial glass dissolution via hydrothermal alteration because the K concentration in the fluid increased up to 40 mmol/kg in the experiments (Figure 3; Table 2). Based on the EPMA results, the analyzed rhyolite contains no K-bearing minerals (e.g., orthoclase) and thus no potential candidate for the main K source for the fluid, except for volcanic glass. Hence, together with the results of SEM observation (Figure 5), it is most likely that the volcanic glass was dissolved and K in the glass was leached into the fluids via hydrothermal alteration. The K depletion in the glass in the rhyolite experiment clearly supports this idea (Figure 8). The present experiments strongly suggest that the glass dissolution is a major controlling factor not only for the high Si concentration but also for the high K concentration in the fluids. The K concentration in the fluid in the rhyolite experiment is higher than that in the andesite experiment (Table 2), and it is consistent with the fact that the K content of rhyolite is higher than that of andesite (Table 1).

The Ca concentration in the fluid monotonously increased up to 3 mmol/kg during the andesite experiment, while the concentration in the rhyolite experiment was relatively low ($<2\ \text{mmol/kg}$) (Table 2). The Ca content of the starting material of andesite was higher than that of rhyolite, and this is consistent with the observation that anorthite is contained only in the andesite. It is likely that the albitization of anorthite via hydrothermal alteration contributed partly to the increased Ca concentration in the fluid in the andesite experiment (Figure 7).

The H_2 concentration in the fluids generally increased during the experiments, particularly in the andesite case (Figure 3). As shown in Section 4, the SEM observations reveal that igneous minerals in the analyzed volcanic rocks did not substantially react with the fluids during the experiments (Figure 5). Considering this, we speculate that ferrous iron in volcanic glass and/or organics contaminated in the natural samples may have been an electron donor in the H_2 generation process. The Fe_2O_3 content of the andesite (9.7%) is higher than in the rhyolite (2.1%), while the loss on ignition (LOI) of the andesite is lower (0.0%) than that of the rhyolite (2.0%) (Table 1). The fact that a larger amount of H_2 was generated in the andesite experiment implies that the main electron donor was ferrous iron rather than contaminated organics. The H_2S concentration in the fluid slightly increased in the andesite experiment. Although the source of sulfur is uncertain, soluble sulfate minerals in the analyzed rock powder should have been removed through cleaning before the experiments. Ferrous iron in the volcanic glass may have also reduced accessory insoluble sulfate in the analyzed volcanic rocks and produced H_2S .

5.3. Comparison with Fluids in the Okinawa Trough

To constrain the major controlling factors of the fluid composition in the natural hydrothermal systems in the Okinawa Trough, we compared the composition of reacted fluids in the present experiments with that of estimated endmember fluids in the trough, especially focusing on their Si concentration. In a natural hydrothermal system, the Si concentration in the fluid has been conventionally measured with two different analytical methods: colorimetry (molybdate-blue method; [53]) and ICP-OES. The concentration of Si ions (SiO_3^{2-}) dissolved into the fluid was measured with the colorimetric method, whereas the bulk Si concentration (including amorphous silica precipitated from the fluid) was analyzed with ICP-OES. During the rapid cooling of the fluid between the in situ sampling at the seafloor vent and the shipboard measurement, some amount of dissolved Si ions in the fluid may precipitate as amorphous silica and polymerize if the pH of the fluid is not adjusted to be alkaline. In such case, even if the on-shipboard measurement is conducted quickly, the Si concentration in the original hydrothermal fluid would be underestimated by the colorimetric measurement [54].

Kawagucci (2015) compiled the chemical composition of hydrothermal fluids in the Okinawa Trough and showed that the estimated Si concentration in the endmember fluids mostly ranges from 11 mM to 13 mM [29]. The compilation with some other data is shown in Figure 9. The Si concentration in the fluid which is in equilibrium with quartz is ~ 13.5 mmol/kg at 325 °C and 150 bar (at the seafloor at a depth of 1500 m) [35] and thus is close to the estimated range of the Si concentration in endmember fluids. Previous studies interpreted that the endmember fluids in the Okinawa Trough are in equilibrium with quartz [20,55]. The lower Si concentrations in some endmember fluids were attributed to the phase separation of the fluid and the rapid discharge of vapor phase from the seafloor before the achievement of re-equilibrium with quartz [22].

Apart from those previous natural observations, the Si concentration in the fluids in the present experiments is up to 30 mM (Figure 3). As discussed above, it is attributed to the substantial dissolution of volcanic glass in the analyzed volcanic rocks and to the buffering by amorphous silica precipitated from the fluids as a precursor of quartz. The Si concentration in the present experimental fluids (up to 30 mM) is substantially higher than the Si concentration in estimated endmember fluids in the Okinawa Trough (Figure 9). This apparent discrepancy could reflect, at least in part, the difference in pressure between the experimental fluids in the reaction cell and the natural fluids at the hydrothermal vents. In the present experiments, the fluids were reacted with rocks at 300 bar, the estimated pressure at the reaction zone in the systems (1000 mbsf at a water depth of 1500 m). On the other hand, the pressure of the fluids at the natural vents is less than 150 bar (at a water depth shallower than 1500 m) in the Okinawa Trough. Hence, some amount of silica would precipitate from the fluids via the pressure decrease during their upwelling from the deeper reaction zone to the discharge zone at the seafloor. However, the pressure contours on the diagram show that the effect of pressure decrease via the fluid rise is too small to explain solely the observed difference in the Si concentration between the experimental and natural fluids (Figure 9). We also infer that the duration of the present experiments (< 2200 h) may have been too short for comparison with natural hydrothermal systems. In fact, as discussed in the former section, the fluids were not in equilibrium with quartz during the experiments, although amorphous silica is metastable at 325 °C and 300 bar. In the natural systems on a much longer time scale, the equilibrium between the fluid and quartz could be achieved in the reaction/discharge zone.

The estimated Si concentration in most endmember fluids (especially with $T_{\text{MAX}} < 250$ °C) in the Okinawa Trough is apparently too high to be explained by the equilibrium with quartz (Figure 9). The apparent deviation from the solubility curve of quartz on the diagram could be attributed to several factors (the inlet in Figure 9). For example, the observed maximum temperature of the fluid (T_{MAX}) is potentially lower than the actual temperature at the reaction zone (T_{R}) in the field. In that case, on the diagram, the point of the fluid is away leftward from the solubility curve of quartz. On the other hand,

the Si concentration in the endmember fluid may have been underestimated when the Si concentration in the natural fluids was measured with colorimetry, as mentioned above. (Indeed, the Si concentration in the natural fluids in the trough was mainly measured with colorimetry (Supplementary Information)). Furthermore, as also mentioned above, the Si concentration in the natural fluid could have been affected by phase separation beneath the seafloor [22]. In addition to these potential factors, we infer that the dissolution of volcanic glass in the surrounding rocks at the reaction zone contributed to the increase in the Si concentration in the natural fluids. The increased Si concentration in the fluid could have been buffered by amorphous silica precipitated from the fluid, as suggested in the present experiments. In summary, the compilation with the present experimental results suggests that the controlling factors of the Si concentration in the hydrothermal fluids in the Okinawa Trough are more complicated than previously assumed.

In addition to the Si concentration, the chemical composition of the fluids in the present experiments is generally inconsistent with that of the estimated endmember fluids in the Okinawa Trough [29]. Three potential mechanisms could explain this apparent discrepancy between the experimental results and natural observations: (1) phase separation, (2) inputs of magmatic volatiles, and (3) hydrothermal reactions with volcanic rocks other than rhyolite and andesite and with sediments. For example, the substantially low Cl and Na concentrations in some endmember fluids in the trough, compared to those in the ambient seawater, are attributed to the subseafloor phase separation [20,22]. The pH values of the fluid at the end of the present experiments (4.5 on rhyolite and 5.5 on andesite) are similar to those of the endmember fluids in the trough, which mostly range between 4.5 and 5.5. However, the pH value in the natural fluids is also influenced by the input of a vapor phase via phase separation and the reaction with sediments. The Ca concentration in the natural fluids is substantially high (up to 20 mM) compared to that in the present experimental fluids (up to 3 mM; Table 2). The high Ca concentration in the natural fluids may be due to reactions with volcanic rocks other than rhyolite and andesite and/or sediments, although the albitization of anorthite via hydrothermal alteration may contribute partly to it, as shown in the present andesite experiment (Figure 7). As discussed in Section 5.1, the K concentration in the fluids in the present experiments is up to 40 mM (Table 2), and we interpret that volcanic glass in the analyzed rhyolite and andesite is the major K source for the fluids. However, the K concentrations in some natural fluids in the Okinawa Trough are much higher, up to 80 mM [56]. In addition to the glass in the volcanic rocks, K-containing minerals (such as K-feldspar, illite, and glauconite) may be another major K source for the natural fluids.

Overall, the chemical composition of the present experimental fluids is generally inconsistent with that of the endmember fluids in the Okinawa Trough [29]. This discrepancy simply reflects the multiple controlling factors of the composition of natural fluids in the back-arc basin setting [5,26]. It is difficult to reproduce such a complex reaction system completely with the simple experimental apparatus in a laboratory. Nevertheless, the present experiments newly emphasize a potential contribution of the dissolution of volcanic glass in intermediate-to-felsic rocks to the fluid composition in the reaction/discharge zone in the trough.

5.4. Global Compilation of Fluid Chemistry in the MOR and ABA Systems

Referring to hydrothermal fields on a global scale, the potential of volcanic glass dissolution and amorphous silica buffering to contribute to the fluid composition is further strengthened (Figure 10). In the MOR hydrothermal systems, it has been widely supposed that the fluid beneath the subseafloor is in equilibrium with minerals in surrounding rocks in the reaction/discharge zone [6,33,57–59]. In particular, the Si concentration in the fluid has been thought to reflect the fluid–quartz equilibrium and has been used to constrain the equilibrium temperature and pressure conditions in the reaction/discharge zone in the system [35]. The observed maximum temperature (T_{MAX}) of the fluid in the mid-ocean ridge hydrothermal systems is up to 370 °C [1], and the Si concentration in the fluid

which is in equilibrium with quartz at 370 °C and 300 bar is estimated to be ~16 mM [35]. The global compilation shows that the estimated Si concentration in the endmember fluids in the MOR systems is mostly along/below quartz solubility curves (Figure 10). Although T_{MAX} constrains the minimum temperature in the seafloor reaction/discharge zone, this observation is consistent with the conventional idea that the fluids are generally in equilibrium with quartz in those systems. A downward deviation from the solubility curves of quartz in some MOR systems could be attributed to phase separation in the reaction/discharge zone [1,35].

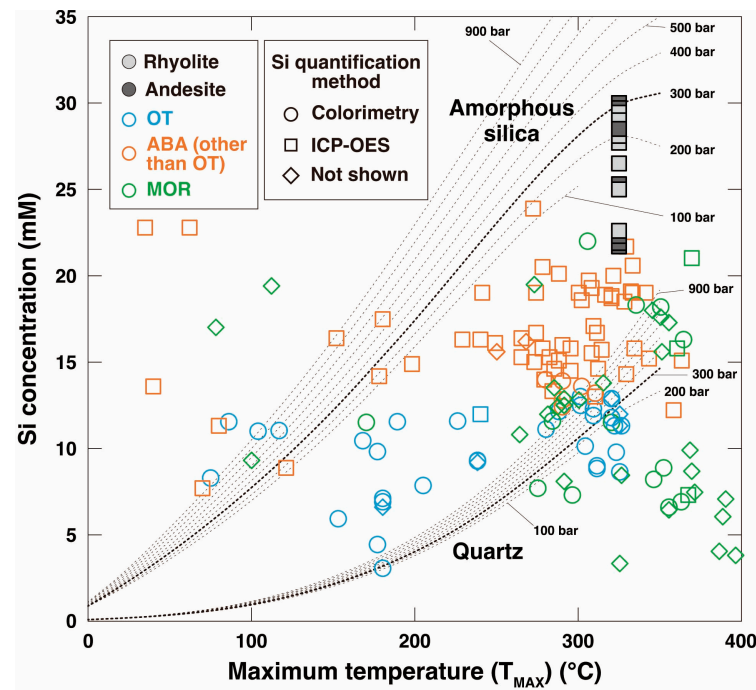


Figure 10. A global compilation of the observed maximum temperature (T_{MAX}) and the estimated Si concentration in the endmember fluids in mid-ocean ridges (MORs) and arc/back-arc (ABA) hydrothermal fields. The solubility curves of quartz and of amorphous silica at 100–900 bar are also shown (dashed). Note that the fluids in the MOR and ABA systems are mostly below and above, respectively, the solubility curves of quartz. OT: Okinawa Trough. References for the compilation are listed in the Supplementary Information (Table S1).

In contrast, the ABA systems are generally characterized by shallow water depth (i.e., low pressure) and low-temperature conditions (limited by the two-phase boundary), compared to the MOR systems [1]. The compilation shows that the Si concentration in the endmember fluids in the ABA systems is mostly above and below the solubility curves of quartz and of amorphous silica, respectively, in the diagram (Figure 10), as seen in the Okinawa Trough (Figure 9). As discussed in Section 5.3, the apparent deviation from the solubility curves of quartz in the diagram could be attributed to several factors. We particularly infer that the dissolution of volcanic glass in surrounding rocks at the reaction zone and the subsequent buffering by amorphous silica precipitated from the fluids contribute, at least in part, to the high Si concentration in the endmember fluids in the ABA systems. Our inference based on the global compilation highlights a fundamental difference between the MOR and ABA hydrothermal systems. The fluids are generally in equilibrium with quartz in the MOR systems, whereas the fluids are mostly in disequilibrium with quartz in the ABA systems. In the ABA systems with relatively low temperatures, amorphous silica (a precursor of quartz) is more stable [35]. Hence, the Si concentration in the fluids may be more effectively buffered by amorphous silica (rather than quartz) compared to in the MOR systems.

5.5. Potential Role of Volcanic Glass/Amorphous Silica in the SMS Deposit Formation

Hydrothermal glass alteration in intermediate-to-felsic volcanic rocks may play an important role in the SMS deposit formation in the Okinawa Trough. Nozaki et al. (2021) recently reported petrological and geochemical characteristics of drill core samples collected from the modern SMS deposit in the middle Okinawa Trough [25]. They revealed the presence of pyrite framboids in close association with altered glass in pumice fragments. According to their scenario, pyrite framboids serve as nuclei at the initial stage and are replaced later by other sulfide minerals to form a large SMS deposit beneath the seafloor.

The present study experimentally demonstrated that volcanic glass in the rhyolite and andesite collected from the trough dissolves substantially and preferentially into the fluids at 325 °C and 300 bar (Figures 3 and 5). This result indicates that volcanic glass in pumice also dissolves substantially into the fluids in the reaction/discharge zone in the natural hydrothermal systems in the trough. The supposed glass dissolution in pumice may facilitate the subsequent void space replacement by sulfides along the scenario of pumice replacement mineralization. The sulfide precipitation was not confirmed in the present experiments as an addition of sulfur species to the experimental system was beyond the scope of the present study focusing on the behavior of silica. Nevertheless, the present results are in line with the model of pumice replacement mineralization in Nozaki et al. (2021) [25].

On the other hand, on the Endeavour Segment of the Juan de Fuca Ridge, Tivey et al. (1999) proposed that the precipitation of amorphous silica from the fluids is a key process for flange growth, stabilizing overhanging ledges, and resultant efficient sulfide precipitation along the edifice [60]. These examples from the Okinawa Trough and the Juan de Fuca Ridge imply that the behavior of silica in water–rock reactions (i.e., the dissolution of glass in the volcanic rocks and the precipitation of amorphous silica from the fluids) is a key to the SMS deposit formation both in MOR and ABA hydrothermal fields. Further observational and experimental studies would emphasize a previously overlooked role of volcanic glass/amorphous silica in the fluid composition and in the formation of associated SMS deposits in both the MOR and ABA fields.

6. Conclusions

To examine the behavior of silica during hydrothermal water–rock reactions, we experimentally reacted fresh rhyolite and andesite rocks collected from the middle and southern Okinawa Trough, respectively, with artificial seawater at 325 °C and 300 bar (the estimated condition at the reaction zone in the fields) over 1800 h. During the experiments, the fluids evolved to be substantially enriched in Si (up to 30 mM), suggesting the substantial dissolution of volcanic glass in the analyzed rocks. The high Si concentration in the fluids cannot be explained by the equilibrium with quartz and was probably buffered by amorphous silica, precipitated from the fluids as a precursor of quartz. The SEM observations with EPMA analyses support the substantial dissolution of volcanic glass in the rocks and the precipitation of amorphous silica from the fluids in the experiments. The present experimental results with a global compilation of natural fluid chemistry in mid-ocean ridge (MOR) and arc/back-arc (ABA) hydrothermal fields suggest that the dissolution of glass in volcanic rocks at the reaction zone and the amorphous silica buffering contribute to the relatively high Si concentration in the fluids in the ABA fields. The present experiments reveal a previously overlooked role of volcanic glass/amorphous silica in the fluid composition in the Okinawa Trough. Our results are also consistent with the model of pumice replacement mineralization for the SMS deposit formation in the trough.

Supplementary Materials: The following supporting information can be downloaded at: <https://www.mdpi.com/article/10.3390/min14030259/s1>, Table S1: Fluid composition in mid-ocean ridge and arc/back-arc hydrothermal fields on a global scale.

Author Contributions: Conceptualization, T.S. (Takazo Shibuya) and K.S.; experiments, M.S. and T.S. (Takazo Shibuya); chemical analyses, M.S., T.S. (Takazo Shibuya), T.S. (Takuya Saito), J.T., H.U. and T.S. (Tomoki Sato); thermodynamic calculations, T.S. (Takazo Shibuya) and H.U.; writing—original

draft preparation, M.S. and T.S. (Takazo Shibuya); writing—review and editing, T.S. (Takuya Saito), J.T., H.U., T.S. (Tomoki Sato) and K.S.; project administration, T.S. (Takazo Shibuya) and K.S.; funding acquisition, M.S. All authors have read and agreed to the published version of the manuscript.

Funding: This research was funded by JSPS KAKENHI (26610159, 15H03740).

Data Availability Statement: The data presented in this study are available on request from the corresponding author.

Acknowledgments: Tatsuo Nozaki provided the analyzed samples and their sampling photos. Yuka Masaki, Naomi Takahashi, and Akiko Makabe assisted with the experiments. Takashi Mikouchi let us use a microscope for lithofacies description and microphotography.

Conflicts of Interest: The authors declare no conflicts of interest.

References

1. Humphris, S.E.; Klein, F. Progress in deciphering the controls on the geochemistry of fluids in seafloor hydrothermal systems. *Ann. Rev. Mar. Sci.* **2018**, *10*, 315–343. [[CrossRef](#)] [[PubMed](#)]
2. Von Damm, K.L. Controls on the chemistry and temporal variability of seafloor hydrothermal fluids. In *Seafloor Hydrothermal Systems: Physical, Chemical, Biological, and Geological Interactions*; Humphris, S.E., Zierenberg, R.A., Mullineaux, L.S., Thomson, R.E., Eds.; Geophysical Monograph Series 95; American Geophysical Union: Washington, DC, USA, 1995; pp. 222–247.
3. Ishibashi, J.; Urabe, T. Hydrothermal activity related to arc-backarc magmatism in the western Pacific. In *Backarc Basins: Tectonics and Magmatism*; Taylor, B., Ed.; Springer: New York, NY, USA, 1995; pp. 451–495.
4. Gamo, T.; Ishibashi, J.; Tsunogai, U.; Okamura, K.; Chiba, H. Unique geochemistry of submarine hydrothermal fluids from arc-back-arc settings of the western Pacific. In *Back-Arc Spreading Systems—Geological, Biological, Chemical, and Physical Interactions*; Christie, D.M., Fisher, C.R., Lee, S.M., Givens, S., Eds.; Geophysical Monograph Series 166; American Geophysical Union: Washington, DC, USA, 2006; pp. 147–161.
5. Nakamura, K.; Takai, K. Theoretical constraints of physical and chemical properties of hydrothermal fluids on variations in chemolithotrophic microbial communities in seafloor hydrothermal systems. *Prog. Earth Planet. Sci.* **2014**, *1*, 5. [[CrossRef](#)]
6. Alt, J.C. Subseafloor processes in mid-ocean ridge hydrothermal systems. In *Seafloor Hydrothermal Systems: Physical, Chemical, Biological, and Geological Interactions*; Humphris, S.E., Zierenberg, R.A., Mullineaux, L.S., Thomson, R.E., Eds.; Geophysical Monograph Series 95; American Geophysical Union: Washington, DC, USA, 1995; pp. 83–114.
7. Seyfried, W.E. Experimental and theoretical constraints on hydrothermal alteration processes at mid-ocean ridges. *Ann. Rev. Earth Planet. Sci.* **1987**, *15*, 317–335. [[CrossRef](#)]
8. Seyfried, W.E.; Bischoff, J.L. Low temperature basalt alteration by seawater: An experimental study at 70 °C and 150 °C. *Geochem. Cosmochim. Acta* **1979**, *43*, 1937–1947. [[CrossRef](#)]
9. Mottl, M.J. Hydrothermal processes at seafloor spreading centers: Application of basalt-seawater experimental results. In *Hydrothermal Processes at Seafloor Spreading Centers*; Rona, P.A., Bostrom, K., Laubier, L., Smith, K.L., Eds.; Springer: New York, NY, USA, 1983; pp. 199–224.
10. Yoshizaki, M.; Shibuya, T.; Suzuki, K.; Shimizu, K.; Nakamura, K.; Takai, K.; Omori, S.; Maruyama, S. H₂ generation by experimental hydrothermal alteration of komatiitic glass at 300 °C and 500 bars: A preliminary result from on-going experiment. *Geochem. J.* **2009**, *43*, e17–e22. [[CrossRef](#)]
11. Shibuya, T.; Yoshizaki, M.; Masaki, Y.; Suzuki, K.; Takai, K.; Russell, M.J. Reactions between basalt and CO₂-rich seawater at 250 and 350 °C, 500 bars: Implications for the CO₂ sequestration into the modern oceanic crust and the composition of hydrothermal vent fluid in the CO₂-rich early ocean. *Chem. Geol.* **2013**, *359*, 1–9. [[CrossRef](#)]
12. Shibuya, T.; Yoshizaki, M.; Sato, M.; Shimizu, K.; Nakamura, K.; Omori, S.; Suzuki, K.; Takai, K.; Tsunakawa, H.; Maruyama, S. Hydrogen-rich hydrothermal environments in the Hadean ocean inferred from serpentinization of komatiites at 300 °C and 300 bars. *Prog. Earth Planet. Sci.* **2015**, *2*, 46. [[CrossRef](#)]
13. Seyfried, W.E.; Ding, K.; Berndt, M.E. Phase equilibria constraints on the chemistry of hot spring fluids at mid-ocean ridges. *Geochem. Cosmochim. Acta* **1991**, *55*, 3559–3580. [[CrossRef](#)]
14. Seyfried, W.E.; Ding, K. Phase equilibria in subseafloor hydrothermal systems: A review of the role of redox, temperature, pH and dissolved Cl on the chemistry of hot spring fluids at midocean ridges. In *Seafloor Hydrothermal Systems: Physical, Chemical, Biological, and Geological Interactions*; Humphris, S.E., Zierenberg, R.A., Mullineaux, L.S., Thomson, R.E., Eds.; Geophysical Monograph Series 95; American Geophysical Union: Washington, DC, USA, 1995; pp. 248–273.
15. Hajash, A.; Chandler, G.W. An experimental investigation of high-temperature interactions between seawater and rhyolite, andesite, basalt and peridotite. *Contrib. Miner. Petrol.* **1981**, *78*, 240–254. [[CrossRef](#)]
16. Shiraki, R.; Sakai, H.; Endoh, M.; Kishima, N. Experimental studies on rhyolite- and andesite-seawater interactions at 300 °C and 1000 bars. *Geochem. J.* **1987**, *21*, 139–148. [[CrossRef](#)]
17. Chiba, H. Chemical modeling of seawater-rock interaction: Effect of rock-type on the fluid chemistry and mineral assemblage. In *Biogeochemical Processes and Ocean Flux in the Western Pacific*; Sakai, H., Nozaki, Y., Eds.; Terra Scientific Publishing Company (TERRAPUB): Tokyo, Japan, 1995; pp. 469–486.

18. Ogawa, Y.; Shikazono, N.; Ishiyama, D.; Sato, H.; Mizuta, T. An experimental study on felsic rock–artificial seawater interaction: Implications for hydrothermal alteration and sulfate formation in the Kuroko mining area of Japan. *Miner. Depos.* **2005**, *39*, 813–821. [[CrossRef](#)]
19. Hannington, M.; Jamieson, J.; Monecke, T.; Petersen, S.; Beaulieu, S. The abundance of seafloor massive sulfide deposits. *Geology* **2011**, *39*, 1155–1158. [[CrossRef](#)]
20. Nakano, A.; Matsumura, M.; Ishibashi, J. Geochemistry of hydrothermal fluids from the Hatoma Knoll in the South Okinawa Trough. *JAMSTEC J. Deep Sea Res.* **2001**, *18*, 139–144.
21. Kishida, K.; Sohrin, Y.; Okamura, K.; Ishibashi, J. Tungsten enriched in submarine hydrothermal fluids. *Earth Planet. Sci. Lett.* **2004**, *222*, 819–827. [[CrossRef](#)]
22. Toki, T.; Itoh, M.; Iwata, D.; Ohshima, S.; Shinjo, R.; Ishibashi, J.; Tsunogai, U.; Takahata, N.; Sano, Y.; Yamanaka, T.; et al. Geochemical characteristics of hydrothermal fluids at Hatoma Knoll in the southern Okinawa Trough. *Geochem. J.* **2016**, *50*, 493–525. [[CrossRef](#)]
23. Toki, T.; Nohara, T.; Urata, Y.; Shinjo, R.; Hokakubo-Watanabe, S.; Ishibashi, J.; Kawagucci, S. Sr isotopic ratios of hydrothermal fluids from the Okinawa Trough and the implications of variation in fluid–sediment interactions. *Prog. Earth Planet. Sci.* **2022**, *9*, 59. [[CrossRef](#)]
24. Halbach, P.; Nakamura, K.; Wahsner, M.; Lange, J.; Sakai, H.; Käselitz, L.; Hansen, R.D.; Yamano, M.; Post, J.; Prause, B.; et al. Probable modern analogue of Kuroko-type massive sulphide deposits in the Okinawa Trough back-arc basin. *Nature* **1989**, *338*, 496–499. [[CrossRef](#)]
25. Nozaki, T.; Nagase, T.; Takaya, Y.; Yamasaki, T.; Otake, T.; Yonezu, K.; Ikehata, K.; Totsuka, S.; Kitada, K.; Sanada, Y.; et al. Subseafloor sulphide deposit formed by pumice replacement mineralization. *Sci. Rep.* **2021**, *11*, 8809. [[CrossRef](#)] [[PubMed](#)]
26. Ishibashi, J.; Ikegami, F.; Tsuji, T.; Urabe, T. Hydrothermal activity in the Okinawa Trough back-arc basin: Geological background and hydrothermal mineralization. In *Subseafloor Biosphere Linked to Hydrothermal Systems: TAIGA Concept*; Ishibashi, J., Okino, K., Sunamura, M., Eds.; Springer: Berlin/Heidelberg, Germany, 2015; pp. 337–359.
27. Sibuet, J.-C.; Hsu, S.-K.; Shyu, C.-T.; Liu, C.-S. Structural and kinematic evolutions of the Okinawa Trough backarc basin. In *Backarc Basins: Tectonics and Magmatism*; Taylor, B., Ed.; Springer: New York, NY, USA, 1995; pp. 343–379.
28. Kikunaga, R.; Song, K.; Chiyonobu, S.; Fujita, K.; Shinjo, R.; Okino, K. Shimajiri Group equivalent sedimentary rocks dredged from sea knolls off Kume Island, central Ryukyus: Implications for timing and mode of rifting of the middle Okinawa Trough back-arc basin. *Island Arc* **2021**, *30*, e12425. [[CrossRef](#)]
29. Kawagucci, S. Fluid geochemistry of high-temperature hydrothermal fields in the Okinawa Trough. In *Subseafloor Biosphere Linked to Hydrothermal Systems: TAIGA Concept*; Ishibashi, J., Okino, K., Sunamura, M., Eds.; Springer: Berlin/Heidelberg, Germany, 2015; pp. 387–403.
30. Ishizuka, H.; Kawanobe, Y.; Sakai, H. Petrology and geochemistry of volcanic rocks dredged from the Okinawa Trough, an active back-arc basin. *Geochem. J.* **1990**, *24*, 75–92. [[CrossRef](#)]
31. Shinjo, R.; Kato, Y. Geochemical constraints on the origin of bimodal magmatism at the Okinawa Trough, an incipient back-arc basin. *Lithos* **2000**, *54*, 117–137. [[CrossRef](#)]
32. Ueda, H.; Shibuya, T.; Sawaki, Y.; Saitoh, M.; Takai, K.; Maruyama, S. Reactions between komatiite and CO₂-rich seawater at 250 and 350 °C, 500 bars: Implications for hydrogen generation in the Hadean seafloor hydrothermal system. *Prog. Earth Planet. Sci.* **2016**, *3*, 35. [[CrossRef](#)]
33. Wetzel, L.R.; Shock, E.L. Distinguishing ultramafic- from basalt-hosted submarine hydrothermal systems by comparing calculated vent fluid compositions. *J. Geophys. Res.* **2000**, *105*, 8319–8340. [[CrossRef](#)]
34. Gallant, R.M.; Von Damm, K.L. Geochemical controls on hydrothermal fluids from the Kairei and Edmond Vent Fields, 23°–25°S, Central Indian Ridge. *Geochem. Geophys. Geosyst.* **2006**, *7*, Q06018. [[CrossRef](#)]
35. Von Damm, K.L.; Bischoff, J.L.; Rosenbauer, R.J. Quartz solubility in hydrothermal seawater: An experimental study and equation describing quartz solubility for up to 0.5 M NaCl solutions. *Am. J. Sci.* **1991**, *291*, 977–1007. [[CrossRef](#)]
36. Gunnarsson, I.; Arnórsson, S. Amorphous silica solubility and the thermodynamic properties of H₄SiO₄ in the range of 0° to 350 °C at P_{sat}. *Geochim. Cosmochim. Acta* **2000**, *64*, 2295–2307. [[CrossRef](#)]
37. Campbell, A.C.; Palmer, M.R.; Klinkhammer, G.P.; Bowers, T.S.; Edmond, J.M.; Lawrence, J.R.; Casey, J.F.; Thompson, G.; Humphris, S.; Rona, P.; et al. Chemistry of hot springs on the Mid-Atlantic Ridge. *Nature* **1988**, *335*, 514–519. [[CrossRef](#)]
38. Charlou, J.L.; Donval, J.P.; Konn, C.; Ondréas, H.; Fouquet, Y.; Jean-Baptiste, P.; Fourré, E. High production and fluxes of H₂ and CH₄ and evidence of abiotic hydrocarbon synthesis by serpentinization in ultramafic-hosted hydrothermal systems on the Mid-Atlantic Ridge. In *Diversity of Hydrothermal Systems on Slow Spreading Ocean Ridges*; Geophysical Monograph Series 188; Rona, P.A., Devey, C.W., Dymont, J., Murton, B.J., Eds.; American Geophysical Union: Washington, DC, USA, 2010; pp. 265–296.
39. Chiba, H.; Ishibashi, J.; Ueno, H.; Oomori, T.; Uchiyama, N.; Takeda, T.; Takamine, C.; Ri, J.; Itomitsu, A. Seafloor Hydrothermal Systems at North Knoll, Iheya Ridge, Okinawa Trough. *JAMSTEC J. Deep Sea Res.* **1996**, *12*, 211–219.
40. Cruse, A.M.; Seewald, J.S.; Sacoccia, P.J.; Zierenberg, R. Hydrothermal fluid composition at Middle Valley, Northern Juan de Fuca Ridge: temporal and spatial variability. In *Magma to Microbe: Modeling Hydrothermal Processes at Oceanic Spreading Centers*; Geophysical Monograph Series 178; Lowell, R.P., Seewald, J.S., Metaxas, A., Perfit, M.R., Eds.; American Geophysical Union: Washington, DC, USA, 2008; pp. 145–166.

41. Ronde, C.E.J.; Massoth, G.J.; Butterfield, D.A.; Christenson, B.W.; Ishibashi, J.; Ditchburn, R.G.; Hannington, M.D.; Brathwaite, R.L.; Lupton, J.E.; Kamenetsky, V.S.; et al. Submarine hydrothermal activity and gold-rich mineralization at Brothers Volcano, Kermadec Arc, New Zealand. *Min. Depos.* **2011**, *46*, 541–584. [[CrossRef](#)]
42. Edmonds, H.N.; German, C.R.; Green, D.R.H.; Huh, Y.; Gamo, T.; Edmond, J.M. Continuation of the hydrothermal fluid chemistry time series at TAG, and the effects of ODP drilling. *Geophys. Res. Lett.* **1996**, *23*, 3487–3489. [[CrossRef](#)]
43. Ishibashi, J.; Tsunogai, U.; Wakita, H.; Watanabe, K.; Kajimura, T.; Shibata, A.; Fujiwara, Y.; Hashimoto, J. Chemical Composition of Hydrothermal Fluids from the Suiyo and the Mokuyo Seamounts, Izu-Bonin Arc. *JAMSTEC J. Deep Sea Res.* **1994**, *10*, 89–97.
44. Jean-Baptiste, P.; Charlou, J.L.; Stievenard, M.; Donval, J.P.; Bougault, H.; Mevel, C. Helium and methane measurements in hydrothermal fluids from the mid-Atlantic ridge: the Snake Pit site at 23° N. *Earth Planet. Sci. Lett.* **1991**, *106*, 17–28. [[CrossRef](#)]
45. Kataoka, S.; Ishibashi, J.; Yamanaka, T.; Chiba, H. Topography and Fluid geochemistry of the Iheya North Knoll seafloor hydrothermal system in the Okinawa Trough. *JAMSTEC J. Deep Sea Res.* **2000**, *16*, 1–7.
46. Mottl, M.J.; Seewald, J.S.; Wheat, C.G.; Tivey, M.K.; Michael, P.J.; Proskurowski, G.; McCollom, T.M.; Reeves, E.; Sharkey, J.; You, C.F.; et al. Chemistry of hot springs along the Eastern Lau Spreading Center. *Geochim. Cosmochim. Acta* **2011**, *75*, 1013–1038. [[CrossRef](#)]
47. Reeves, E.P.; Seewald, J.S.; Saccocia, P.; Bach, W.; Craddock, P.R.; Shanks, W.C.; Sylva, S.P.; Walsh, E.; Pichler, T.; Rosner, M. Geochemistry of hydrothermal fluids from the PACMANUS, Northeast Pual and Vienna Woods hydrothermal fields, Manus Basin, Papua New Guinea. *Geochim. Cosmochim. Acta* **2011**, *75*, 1088–1123. [[CrossRef](#)]
48. Seyfried, W.E.; Pester, N.J.; Ding, K.; Mikaella Rough, M. Vent fluid chemistry of the Rainbow hydrothermal system (36 N, MAR): Phase equilibria and in situ pH controls on subseafloor alteration processes. *Geochim. Cosmochim. Acta* **2011**, *75*, 1574–1593. [[CrossRef](#)]
49. Von Damm, K.L. Chemistry of hydrothermal vent fluids from 9°–10°N, East Pacific Rise: “Time zero,” the immediate post-eruptive period. *J. Geophys. Res.* **2000**, *105*, 11203–11222. [[CrossRef](#)]
50. Von Damm, K.L.; Edmond, J.M.; Grant, B.; Measures, C.I.; Walden, B.; Weiss, R.F. Chemistry of submarine hydrothermal solutions at 21° N, East Pacific Rise. *Geochim. Cosmochim. Acta* **1985**, *49*, 2197–2220. [[CrossRef](#)]
51. Von Damm, K.L.; Edmond, J.M.; Measures, C.I.; Grant, B. Chemistry of submarine hydrothermal solutions at Guaymas Basin, Gulf of California. *Geochim. Cosmochim. Acta* **1985**, *49*, 2221–2237. [[CrossRef](#)]
52. Kikuchi, S.; Shibuya, T.; Abe, M.; Uematsu, K. Experimental chondrite–water reactions under reducing and low-temperature hydrothermal conditions: Implications for incipient aqueous alteration in planetesimals. *Geochim. Cosmochim. Acta* **2022**, *319*, 151–167. [[CrossRef](#)]
53. Gieskes, J.M.; Gamo, T.; Brumsack, H. *Chemical Methods for Interstitial Water Analysis Aboard JOIDES Resolution*; Technical Note 15; Texas A&M University: College Station, TX, USA, 1991; Volume 15, pp. 1–60.
54. Strickland, J.D.H.; Parsons, T.R. *A Practical Handbook of Seawater Analysis*; Fisheries Research Board of Canada: Ottawa, ON, Canada, 1968; pp. 65–70.
55. Ishibashi, J.; Noguchi, T.; Toki, T.; Miyabe, S.; Yamaguchi, S.; Onishi, Y.; Yamanaka, T.; Yokoyama, Y.; Omori, E.; Takahashi, Y.; et al. Diversity of fluid geochemistry affected by processes during fluid upwelling in active hydrothermal fields in the Izena Hole, the middle Okinawa Trough back-arc basin. *Geochem. J.* **2014**, *48*, 1–13. [[CrossRef](#)]
56. Kawagucci, S.; Chiba, H.; Ishibashi, J.; Yamanaka, T.; Toki, T.; Muramatsu, Y.; Ueno, Y.; Makabe, A.; Inoue, K.; Yoshida, N.; et al. Hydrothermal fluid geochemistry at the Iheya North field in the mid-Okinawa Trough: Implication for origin of methane in subseafloor fluid circulation systems. *Geochem. J.* **2011**, *45*, 109–124. [[CrossRef](#)]
57. Alt, J.C.; Honnorez, J.; Laverne, C.; Emmermann, R. Hydrothermal alteration of a 1 km section through the upper oceanic crust, Deep Sea Drilling Project Hole 504B: Mineralogy, chemistry, and evolution of seawater–basalt interactions. *J. Geophys. Res.* **1986**, *91*, 10309–10335. [[CrossRef](#)]
58. Bowers, T.S.; Taylor, H.P. An integrated chemical and stable-isotope model of the origin of midocean ridge hot spring systems. *J. Geophys. Res.* **1985**, *90*, 12583–12606. [[CrossRef](#)]
59. Bowers, T.S.; Campbell, A.C.; Measures, C.I.; Spivack, A.J.; Khadem, M.; Edmond, J.M. Chemical controls on the composition of vent fluids at 13°–11°N and 21°N, East Pacific Rise. *J. Geophys. Res.* **1988**, *93*, 4522–4536. [[CrossRef](#)]
60. Tivey, M.K.; Stakes, D.S.; Cook, T.L.; Hannington, M.D.; Petersen, S. A model for growth of steep-sided vent structures on the Endeavour Segment of the Juan de Fuca Ridge: Results of a petrologic and geochemical study. *J. Geophys. Res.* **1999**, *104*, 22859–22883. [[CrossRef](#)]

Disclaimer/Publisher’s Note: The statements, opinions and data contained in all publications are solely those of the individual author(s) and contributor(s) and not of MDPI and/or the editor(s). MDPI and/or the editor(s) disclaim responsibility for any injury to people or property resulting from any ideas, methods, instructions or products referred to in the content.